Applied Clay Science 186 (2020) 105429

Contents lists available at ScienceDirect

Applied Clay Science

journal homepage: www.elsevier.com/locate/clay

Research Paper

One-pot synthesis of the reduced-charge montmorillonite via molten salts treatment

Qiuzhi He[a,b,c], Runliang Zhu[a,b,c,*], Qingze Chen[a,b,c], Yanping Zhu[a,b,c], Yixuan Yang[a,b,c], Jing Du[a,b,c], Jianxi Zhu[a,b,c], Hongping He[a,b,c]

[a] CAS Key Laboratory of Mineralogy and Metallogeny, Guangdong Provincial Key Laboratory of Mineral Physics and Materials, Guangzhou Institute of Geochemistry, Chinese Academy of Sciences, Guangzhou 510640, China
[b] University of Chinese Academy of Sciences, Beijing 100049, China
[c] Institutions of Earth Science, Chinese Academy of Sciences, Beijing 100029, China

ARTICLE INFO

Keywords:
Clay minerals
Reduced-charge
Montmorillonite
Molten salt

ABSTRACT

Layer charge is a critical factor determining the structural characteristics and physicochemical properties of clay minerals, and fixing small cations (e.g., Li^+) into the tetrahedral/octahedral sheets of clay minerals is a feasible way for reducing their layer charges. However, conventional methods for preparing reduced-charge clay minerals are usually quite complex and time-consuming. Herein, a facile one-pot treatment method for preparing reduced-charge clay minerals was successfully developed using molten salts. In particular, montmorillonite (Mt) was mixed with mono $LiNO_3$ or $LiNO_3$-$NaNO_3$ mixture, which was then heated above the melting points of salts. The obtained results showed that the cation exchange capacity (CEC) of Mt decreased evidently after being treated with molten $LiNO_3$, and the CEC value was reversely related to the heating time. The X-ray diffraction results demonstrated that Mt layers collapsed upon treatment with molten $LiNO_3$. On the other hand, the partial replacement of $LiNO_3$ by $NaNO_3$ could restrict the collapse of Mt layers, as the larger ionic radius of Na^+ (than Li^+) helped in maintaining the interlayer spaces of Mt during the process of charge reduction. As indicated by the Fourier transform infrared spectroscopy, the structural OH stretching vibration shifted to a higher wavenumber (from 3623 to 3632 cm^{-1}) after the molten $LiNO_3$ treatment, which suggested that some Li^+ ions migrated into the hexagonal cavities in the tetrahedral sheets of Mt, and the new band at 3670 cm^{-1} indicated that some Li^+ ions even further migrated into the octahedral vacancies of Mt. The locations of fixed Li^+ ions were further confirmed by the X-ray photoelectron spectroscopy characterization. Due to the migration of Li^+ ions into the layers of Mt, the Li1s peak shifted to lower binding energy. The above results showed that the molten salt treatment might be a cost-effective and environmentally friendly approach for synthesizing reduced-charge clay minerals, and using mixed molten salts can help in maintaining the interlayer structure.

1. Introduction

Clay minerals are hydrated aluminosilicates consisting of one tetrahedral sheet connected to an octahedral sheet (for 1:1 type) or two inward-point tetrahedral silicate sheets sandwiching one octahedral sheet (for 2:1 type). The non-equivalent isomorphous substitutions of Al^{3+} by Mg^{2+}/Fe^{2+} in the octahedral sheet and Si^{4+} by Al^{3+} in tetrahedral sheets generate negative charges on aluminosilicates layers, which are balanced by exchangeable cations (Bergaya and Lagaly, 2013; Wu et al., 2014; Zhou et al., 2019). Consequently, clay minerals possess unique physicochemical properties (e.g., cation exchange and swelling capacities) (Zhou, 2011; Ma et al., 2016).

Montmorillonite (Mt) is a typical 2:1 clay mineral. As an intrinsic nature of Mt, its layer charge greatly influences the physical and chemical properties of Mt, such as cation exchange capacity (CEC), layer stacking order and swelling capacity (Christidis et al., 2006; Zemanová et al., 2006; Skoubris et al., 2013). Over the past decades, numerous studies have shown that the layer charge reduction can be an effective approach in modifying the properties of Mt. For instance, it leads to the decrease of amounts of interlayer cations, which can increase the distance among the cations, providing more accessible interlayer spaces. In addition, the reduction of layer charge can also decrease the swelling capacity of Mt (Chorom and Rengasamy, 1996). Noticeably, it can also extend the application fields for Mt (Czímerová et al., 2008; Luo et al.,

* Corresponding author.
E-mail address: zhurl@gig.ac.cn (R. Zhu).

https://doi.org/10.1016/j.clay.2019.105429
Received 26 September 2019; Received in revised form 24 December 2019; Accepted 26 December 2019
Available online 14 January 2020

2014). For example, organo-Mt synthesized by modifying the reduced-charge Mt (RC-Mt) with organic cations showed much higher adsorption capacity for organic contaminant than the sample synthesized using raw Mt (Zhu et al., 2007b; Ruan et al., 2008; Pálková et al., 2009; Luo et al., 2015; Barrientos-Velázquez et al., 2016; Zhu et al., 2016). Besides, after the intercalation of inorganic polycations and thermal treatment, RC-Mt with a porous structure could be developed, which exhibited high catalytic activities in various catalytic reactions, e.g., alkylation, disproportionation and dehydrogenation of organic (Gil et al., 2000; Sychev et al., 2000; Mishra and Rao, 2004; Wang et al., 2015).

A conventional method for preparing RC-Mt is as follows: Mt containing small-sized exchangeable cations (e.g., Li^+, Cu^{2+}, and Ni^{2+}) within the interlayer spaces is prepared in a solution through repeated cation exchange and subsequent washing and centrifugation. Then, the collected supernatant samples are heated at 100–300 °C for several hours, and the cations can migrate from the interlayer spaces into the Mt layers, partially neutralizing the negative charge on the layers (Ormerod and Newman, 1983; Jaynes et al., 1992 ; Purnell and Yun, 1993; Madejová et al., 1999; Bujdák et al., 2001). This method requires complex steps (e.g., repeated cation exchange reaction, washing, and a long period of thermal treatment), which results in the consumption of a long time and large amounts of the water resource and hinders the practical applications of RC-Mt (Clementz and Mortland, 1974; Komadel, 2003). Other studies, therefore, have been proposed to deal with these shortcomings (Ebina et al., 1999; Zemanová et al., 2006). For example, microwave heating was applied to shorten the heating time to just several minutes (Zitnan et al., 2009). Despite this progress, the complex process for the preparation of small-sized cations saturated Mt is still inevitable. In this term, developing more effective, simplified, and environmentally friendly methods for preparing RC-Mt is highly desired.

The synthesis method based on molten salts has been considered as a cost-effective approach in preparing various nanomaterials (e.g., carbon and silicon nanomaterials) (Deng et al., 2015; Chen et al., 2018; Chen et al., 2019; Sun et al., 2019). Molten salts can provide a liquid environment with a high concentration of non-hydrated ions, and can easily penetrate into porous materials (Hu et al., 2017; Zhang et al., 2019). Moreover, White (1954) found that when muscovite was heated with molten lithium nitrate at 300 °C, Li^+ replaces K^+ in the interlayer, and then enters the lattice, which renders the muscovite expandable ability. Theoretically, the non-hydrated cations of small size (e.g., Li^+) can simultaneously migrate into the Mt layers under the high-temperature treatment. As a result, the treatment of Mt using molten salts containing small cations (e.g., $LiNO_3$) should be able to obtain RC-Mt. On the other hand, previous studies using the conventional method of reduction of layer charge showed that the migration of small cations induced by thermal treatment can be heterogeneous because of the uneven distribution of layer charge, which subsequently causes the collapse of some Mt layers (Alvero et al., 1994; Zhu et al., 2014). To restrict the collapse of Mt layers, our group proposed a partial replacement of interlayer Li^+ ions with organic cations, as the organic cations cannot migrate into the Mt layers and will act as 'pillars' to maintain the interlayer spaces (Zhu et al., 2014). Similarly, we proposed that the interlayer spaces of Mt can be well maintained by using mixed molten salts containing both small and large-sized inorganic cations (e.g., Li^+ and Na^+).

In this work, we reported a one-pot synthesis strategy for the successful preparation of RC-Mt which was obtained by heating the mixture of Mt and molten salt (i.e., mono $LiNO_3$ or $LiNO_3$-$NaNO_3$ mixture) at 260 °C. The structural characteristics and CEC of the resulting RC-Mt were characterized. In addition, the related mechanisms for charge reduction were also studied. The obtained results of this work well showed that the molten salt method is rather effective, and the interlayer spaces can be well obtained. This method should be applicable to the large-scale production of RC-Mt.

2. Experiments

2.1. Materials

The raw Mt was calcium-rich (Ca-Mt, purity > 95%) and collected from Inner-Mongolia. The structural formula of Mt is $(Ca_{0.2}Na_{0.01}K_{0.01}Mg_{0.05})(Si_{3.94}Al_{0.06})(Al_{1.23}Mg_{0.46}Fe_{0.27})O_{10}(OH)_2{\cdot}nH_2O$. The permanent layer charge of Mt is 0.52 per formula unit (e.g., 0.06 in tetrahedral and 0.46 in octahedral). According to the method of adsorption of $[Co(NH_3)_6]^{3+}$ proposed by Zhu et al. (2007), the CEC of Ca-Mt estimated in this study is 1.15 mmol/g. $LiNO_3$ and $NaNO_3$ were obtained from Shanghai Aladdin biochemical technology Co. China. All chemical reagents were used as received without any further treatment.

2.2. Preparation of RC-Mt

2.2.1. Preparation of RC-Mt by molten $LiNO_3$

0.0575 mol $LiNO_3$ was manually ground with 1 g Ca-Mt in an agate mortar for 10 min. The mixed powder was transferred into a crucible and then heated at 260 °C for 1, 1.5, 2, 3, 5, 10, and 20 h, respectively. After cooling to room temperature, the obtained products were rinsed with ultra-pure water to remove residual $LiNO_3$, and then freeze-dried for 24 h. For clarity, the samples were labeled as Li-Mt-s (s = 1, 1.5, 2, 3, 5, 10, and 20 h).

2.2.2. Preparation of RC-Mt by molten $LiNO_3$-$NaNO_3$ mixture

$LiNO_3$ and $NaNO_3$ were first uniformly mixed with different molar ratios of Li^+ and Na^+ ions (Li^+: Na^+ = 5:5, 7:3, and 8:2), and the total number of the mixed salt was 0.0575 mol. Then, the mixed salt was further combined with Ca-Mt (1 g) and ground in a mortar for 10 min. Subsequently, the solid was calcined in an oven at 260 °C for 1, 1.5, 2, 3, 5, 10, and 20 h, respectively. Then, the final mixture was cooled to room temperature. The resulting samples were rinsed with ultra-pure water and freeze-dried for 24 h. For clarity, when the molar ratio of Li^+ and Na^+ was 7:3, the samples were denoted as 7Li/3Na-Mt-s (s = 1, 1.5, 2, 3, 5, 10, and 20 h). When the molar ratio of Li^+ and Na^+ was 5:5 and 8:2, the samples were denoted as 5Li/5Na-Mt-s and 8Li/2Na-Mt-s (s = 5, 10, and 20 h), respectively.

2.3. The hydration experiment of RC-Mt

1 g of RC-Mt sample was added into 50 mL distilled water, and then the resulting mixture was shaken at room temperature for 24 h, which provided enough time to hydrate the cations in the interlayers of RC-Mt. After centrifugation and freeze-dring for 24 h, the products were obtained and donated as Li-Mt-s-w and 7Li/3Na-Mt-s-w, respectively.

2.4. Characterization methods

The CEC values of all samples were determined according to the method proposed by Zhu et al. (2007). Briefly, 1 g RC-Mt powder sample was added into 20 mL $[Co(NH_3)_6]Cl$ solution with a concentration of 25 mmol/L, and the resulting mixture was shaken at 25 °C for 24 h. After centrifugation, the concentration of $[Co(NH_3)_6]Cl$ in the supernatant was determined using a UV-VIS spectrophotometer at a wavelength of 472 nm. Subsequently, the CEC values were estimated by the differences between the initial and equilibrium concentrations.

X-ray diffraction (XRD) results of all samples were determined by a Bruker D8 Advance X-ray diffractometer. The measurements were operated with Ni-filtered Cu Kα radiation (40 kV and 40 mA), and patterns were recorded over the 2θ range of 3–24° with a scanning speed of 3°/min. The basal spacings were determined from 2θ values of the corresponding basal reflection.

Fourier transform infrared (FTIR) spectroscopy characterization was performed using the KBr pressed pellet method with a Brucker Vertex-

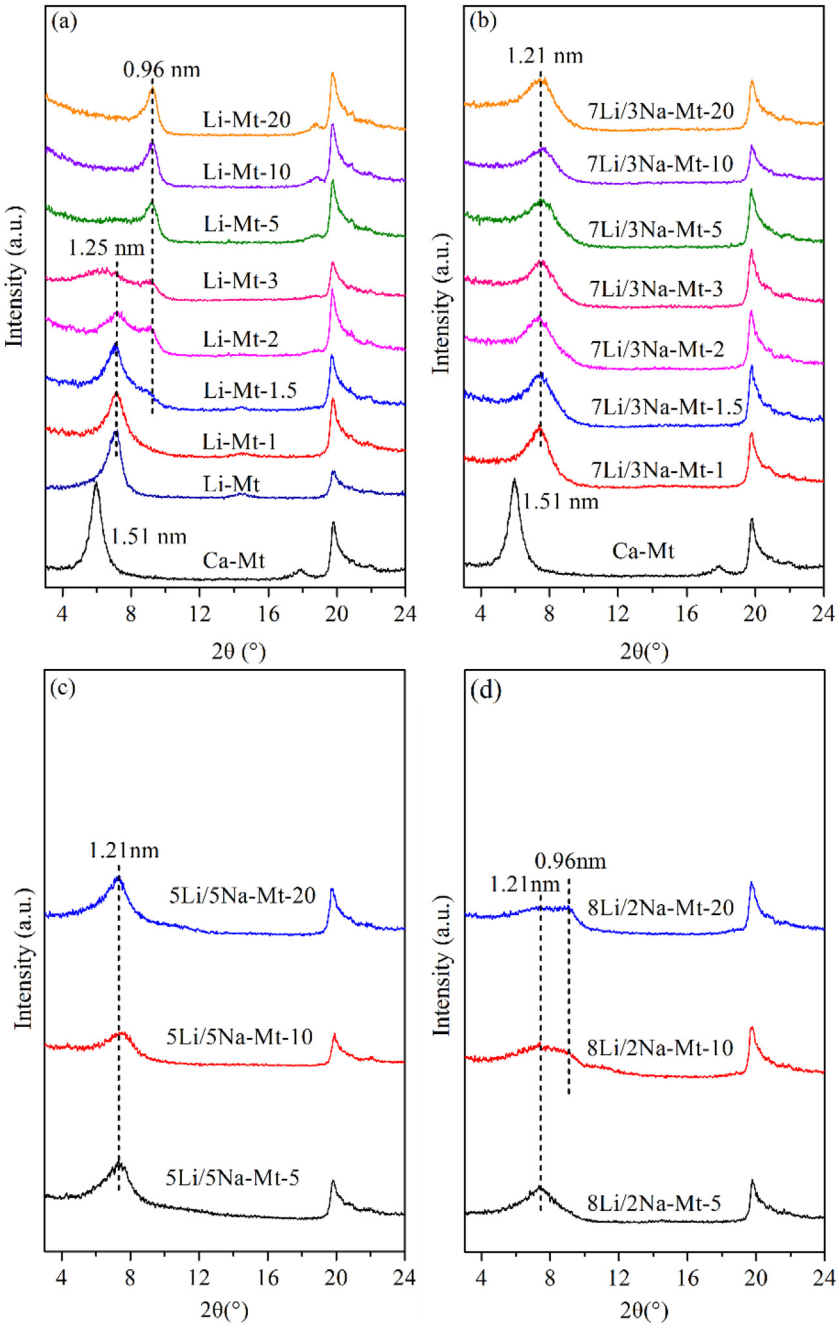

Fig. 1. The XRD patterns of Li-Mt-s (a), 7Li/3Na-Mt-s (b), 5Li/5Na-Mt-s (c), and 8Li/2Na-Mt-s (d), respectively. Li-Mt represents the Mt treated with molten $LiNO_3$ at 260 °C for 5 min. Li-Mt-1, Li-Mt-1.5, Li-Mt-2, Li-Mt-3, Li-Mt-5, Li-Mt-10, and Li-Mt-20 represent the Mt treated with molten $LiNO_3$ at 260 °C for 1, 1.5, 2, 3, 5, 10, and 20 h, respectively. 7Li/3Na-Mt-1, 7Li/3Na-Mt-1.5, 7Li/3Na-Mt-2, 7Li/3Na-Mt-3, 7Li/3Na-Mt-5, 7Li/3Na-Mt-10, and 7Li/3Na-Mt-20 represent the Mt treated with molten $LiNO_3$-$NaNO_3$ mixture at 260 °C for 1, 1.5, 2, 3, 5, 10, and 20 h, respectively. 5Li/5Na-Mt-5, 5Li/5Na-Mt-10, and 5Li/5Na-Mt-20 represent the Mt treated with molten $LiNO_3$-$NaNO_3$ mixture at 260 °C for 5, 10 and 20 h, respectively. 8Li/2Na-Mt-5, 8Li/2Na-Mt-10, and 8Li/2Na-Mt-20 represent the Mt treated with molten $LiNO_3$-$NaNO_3$ mixture at 260 °C for 5, 10 and 20 h, respectively.

70 FTIR spectrophotometer. The spectra were recorded at room temperature with a resolution of 4.0 cm^{-1} over the range of 4000–400 cm^{-1}. Data analysis was performed by the OPUS software.

X-ray photoelectron spectroscopy (XPS) measurements were carried out, using a Thermo Fisher Scientific K-Alpha spectrometer with a monochromatic Al X-ray source of 100 W, and the C1s from the surface adventitious carbon with a binding energy of 248.8 eV was taken as a reference.

3. Results and discussion

3.1. XRD characterization

In Fig. 1a, the d_{001}-value of 1.51 nm for the Ca-Mt was shown, corresponding to Ca^{2+} with two H_2O layers within the interlayer spaces of Mt (Chen et al., 2017). After the treatment with molten $LiNO_3$, the resulting RC-Mt showed different basal spacings. Specifically, the basal spacing of Li-Mt-s reached 1.25 nm even when the heating time is only 5 min, suggesting that Ca^{2+} ions were rapidly exchanged by Li^+ ions in the molten salt system (in this term, the sample heated for 5 min was denoted as Li-Mt). As the heating time increased, a new reflection corresponding to the basal spacing of 0.96 nm for Li-Mt-1.5, Li-Mt-2, and Li-Mt-3 was shown, indicating the collapse of some Mt layers. This result is attributed to the uneven migration of Li^+ ions into the Mt layers, a similar phenomenon was observed in conventional methods of reduction of layer charge. As the heating time further increased to 5 h, only the d_{001}-value of 0.96 nm was shown, which indicates the complete collapse of Mt layers (Chen et al., 2017).

To restrict the collapse of Mt layers, Ca-Mt was treated with the molten $LiNO_3$-$NaNO_3$ mixture (a molar ratio of 7:3 for Li^+ and Na^+). The XRD patterns of 7Li/3Na-Mt-s heated from 1 to 20 h were obtained (Fig. 1b). The reflection corresponding to the basal spacing of 1.21 nm

was shown, indicating no collapse of Mt layers for 7Li/3Na-Mt-s. This phenomenon should be attributed to the existence of Na^+ in the interlayer space, as the Na^+ with a large radius cannot migrate into Mt layers, acting as 'pillars' to hinder the collapse of Mt layers during thermal treatment. Similar finding was observed in Bergaya et al. (1979): heating bi-ionic (Li^+ + Na^+) Mt (prepared by mixing different volumes of Na- and Li-saturated Mt) at 240 °C for 24 h, the Li^+ ions migrated into the layers of Mt while Na^+ ions could be exchanged by other cations. We also noticed that the ratio of Li^+ and Na^+ ions in the mixed molten salts can significantly affect the collapse inhibiting capacity. For example, 5Li/5Na-Mt-s could well retain their interlayer spaces (Fig. 1c). In contrast, the layers of 8Li/2Na-Mt-s collapsed when the thermal treatment at 260 °C lasted over 10 h, possibly resulting from an insufficient amount of Na^+ ions within the interlayer spaces of Mt to maintain the interlayer spaces (Fig. 1d). The above results indicate the importance of using an appropriate molar ratio of Li^+ ions and Na^+ ions in the mixed molten salts, which can affect the collapse inhibiting the capacity of Mt interlayer.

3.2. Change of cation exchange capacity

As expected, with the increase of heating time, the CEC values of Li-Mt-s, 7Li/3Na-Mt-s decreased (Fig. 2) and the efficiency of reduction for layer charge (i.e., the decreased CEC value/the original CEC value) decreased for all the samples. However, the efficiency of the reduction of Li-Mt-s is higher than that of 7Li/3Na-Mt-s (Fig. 2). Specifically, when the heating time was 5 h, the CEC value of Li-Mt-5 decreased extensively to 26.9% of the original value of Ca-Mt, while that of 7Li/3Na-Mt-5 only decreased to 55.6%. We also found that the ratio of Li^+ and Na^+ ions in the mixed molten salts can significantly affect the efficiency of reduction for layer charge. For example, 5Li/5Na-Mt-5 (to 76.5% of the original value) and 8Li/2Na-Mt-5 (to 45.2% of the original value) (Table 1). As the heating time further increased, only a slight change in CEC value was observed for Li-Mt-s, 7Li/3Na-Mt-s, 5Li/5Na-Mt-s, and 8Li/2Na-Mt-s. The above results indicate that the treatment of Mt with molten $LiNO_3$ could achieve a rapid decrease of layer charge, while the partial replacement of $LiNO_3$ by $NaNO_3$ could weaken the efficiency of reduction for layer charge.

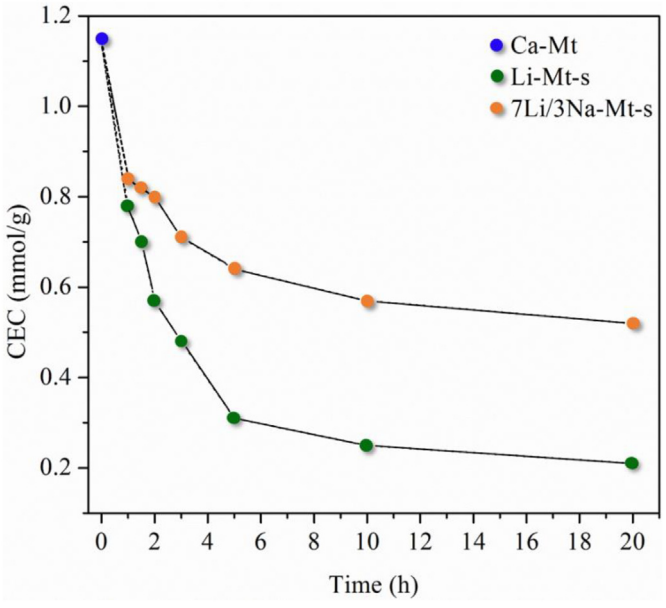

Fig. 2. Effect of heating time on the CEC of Li-Mt-s and 7Li/3Na-Mt-s, respectively.

Table 1
The CEC values of Li-Mt-s, 5Li/5Na-Mt-s, 7Li/3Na-Mt-s, and 8Li/2Na-Mt-s heated for 5, 10, and 20 h, respectively.

Time (h)	CEC (mmol/g)			
	Li-Mt-s	5Li/5Na-Mt-s	7Li/3Na-Mt-s	8Li/2Na-Mt-s
5	0.31	0.88	0.64	0.52
10	0.25	0.80	0.57	0.47
20	0.21	0.80	0.52	0.37

3.3. FTIR spectroscopy characterization

FTIR spectroscopy was used to examine the structural changes in Li-Mt-s and 7Li/3Na-Mt-s (Fig. 3). The broad absorption band at 3621 cm^{-1} for raw Ca-Mt is assigned to the stretching vibrations of structural OH groups and the O-H band of H_2O (Pálková et al., 2003; Kuligiewicz et al., 2015). With the increase of heating time, the absorption band at 3621 cm^{-1} gradually shifted to higher wavenumbers (i.e., from 3623 to 3632 cm^{-1} for Li-Mt-s and to 3628 cm^{-1} for 7Li/3Na-Mt-s) (Fig. 3a and c). These shifts of absorption band should be induced by the partial migration of Li^+ ions from interlayer spaces into the hexagonal cavities of the tetrahedral sheets. Similar results were also observed by Madejová et al. (2000) during the heating of Li-exchanged Mt (prepared by repeated cation exchange in solution). Additionally, a new absorption band near 3670 cm^{-1} in the spectra of Li-Mt-2 and 7Li/3Na-Mt-5 corresponding to the stretching vibration of AlMgLiOH was observed, which should be ascribed to the migration of Li^+ ions into the vacant octahedral sites (Srasra et al., 1994; Madejová et al., 2000). As the heating time increased, the intensity of the AlMgLiOH stretching band gradually became obvious (Fig. 3a and c), implying an increasing amount of migrated Li^+ ions. This phenomenon is consistent with the finding by Madejová et al. (2006): the intensity of the AlMgLiOH stretching band gradually rose with increasing the amounts of the Li^+ ions. However, the intensity of the AlMgLiOH stretching band was much weaker than that reported in Madejová et al. (2006), which might be induced by the residual Ca^{2+} in the interlayers of Mt hindering the migration of Li^+. The quality of the data allows for the second derivative analysis (Fig. S1). Combining the measured CEC values with the FTIR characterization results, one can tell that thermal treatment induced significant migration of interlayer Li^+ ions into the layers of Mt in this molten salt treatment system, and the hexagonal cavities on tetrahedral sheets and the vacant sites on octahedral sheets are the locations of fixed Li^+ ions.

The absorption band at 1036 cm^{-1} for raw Mt arises from Si-O stretching vibrations in the tetrahedral sheet, which shifted to higher wavenumbers (i.e., from 1036 to 1053 cm^{-1} for Li-Mt-s and to 1047 cm^{-1} for 7Li/3Na-Mt-s) (Fig. 3b and d). In addition, a new absorption band appeared at 1116 cm^{-1} for both Li-Mt-s and 7Li/3Na-Mt-s, indicating that the structure of Mt becomes more pyrophyllite-like (Komadel et al., 2003; Chen et al., 2017). The absorption bands located at 915 and 841 cm^{-1} are attributed to the bending vibrations of AlAlOH and AlMgOH, respectively. A slight shift of AlAlOH bending vibrations was observed for Li-Mt-s (i.e., from 915 to 925 cm^{-1}) and 7Li/3Na-Mt-s (i.e., from 915 to 922 cm^{-1}), respectively. These results are well in agreement with the changes in CEC values, and the reduction of layer charge is faster for Li-Mt-s than that for 7Li/3Na-Mt-s (Fig. 2).

3.4. X-ray photoelectron spectroscopy characterization

The XPS characterization was carried out to elucidate the locations of migrated Li^+ ions on Li-Mt-s and 7Li/3Na-Mt-s. The high-resolution Li1s XPS spectra could be deconvoluted into three components at the binding energies of approximately 57.1, 56.6, and 55.4 eV (Fig. 4a and b). We noticed that the binding energy of Li1s was shown at

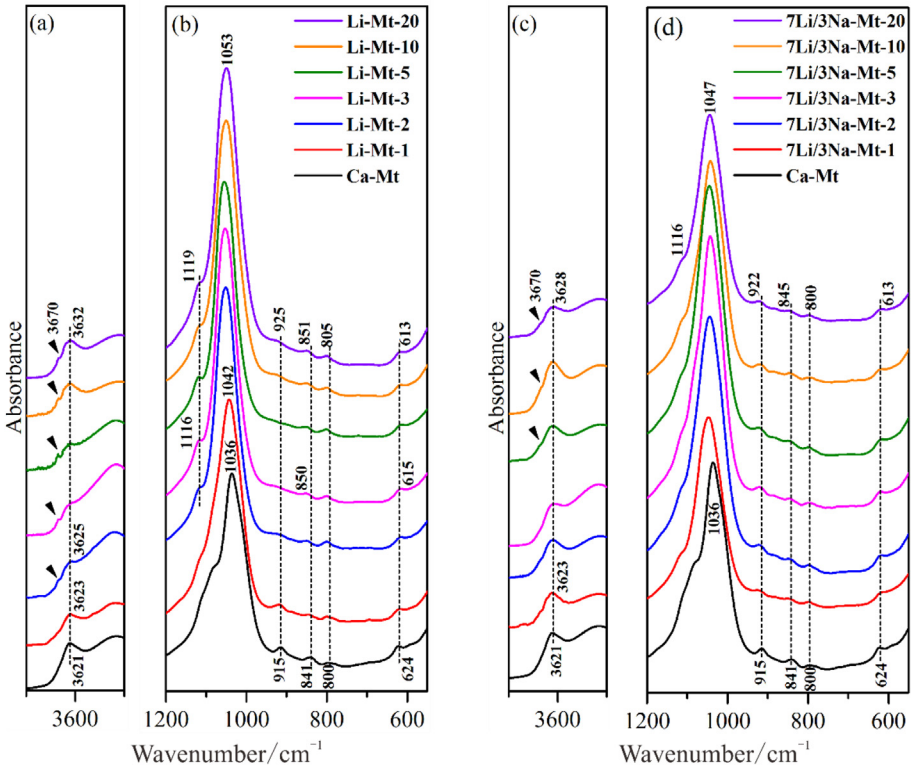

Fig. 3. FTIR spectra of Li-Mt-s (a and b) and 7Li/3Na-Mt-s (c and d), respectively. Li-Mt-1, Li-Mt-2, Li-Mt-3, Li-Mt-5, Li-Mt-10, and Li-Mt-20 represent the Mt treated with molten $LiNO_3$ at 260 °C for 1, 2, 3, 5, 10, and 20 h, respectively. 7Li/3Na-Mt-1, 7Li/3Na-Mt-2, 7Li/3Na-Mt-3, 7Li/3Na-Mt-5, 7Li/3Na-Mt-10, and 7Li/3Na-Mt-20 represent the Mt treated with molten $LiNO_3$-$NaNO_3$ mixture at 260 °C for 1, 2, 3, 5, 10, and 20 h, respectively.

approximately 57.1 eV for the Li-Mt-s heated for only 5 min, and the binding energy of Li1s is consistent with that of the unheated Li-exchanged Mt (prepared by repeated cation exchange in LiCl solution) in which the Li^+ ions located in the interlayer spaces (Theng et al., 1997). Consequently, the Li1s peak found in this study should be attributed to the existence of the Li^+ ions within the interlayer spaces. After heating at 260 °C for 1 h, the broadened Li1s peak shifted to lower binding energy for both Li-Mt-s and 7Li/3Na-Mt-s. In addition, a new Li1s peak appeared at approximately 56.6 eV is attributed to the migration of Li^+ ions into the hexagonal cavities of the tetrahedral sheets (Theng et al., 1997). As the heating time further increased to 20 h, a new peak at the binding energy of approximately 55.4 eV was observed, and this binding energy is well in agreement with that of hectorite in which the Li^+ ions occupy the octahedral sites (Theng et al., 1997). Moreover, the previous study of density functional theory calculations (Ebina et al., 1999) proposed that the migration of Li^+ ions from the hexagonal cavities sites to vacant octahedral sites is favorable, since the calculated Li1s binding energy in the octahedral sites is lower than that in the hexagonal cavities sites. Therefore, the new peak of Li1s appeared at approximately 55.4 eV should be assigned to the Li^+ ions located in the octahedral sites. The above results indicate that a part of Li^+ ions has migrated from the hexagonal cavities into the octahedral vacancies

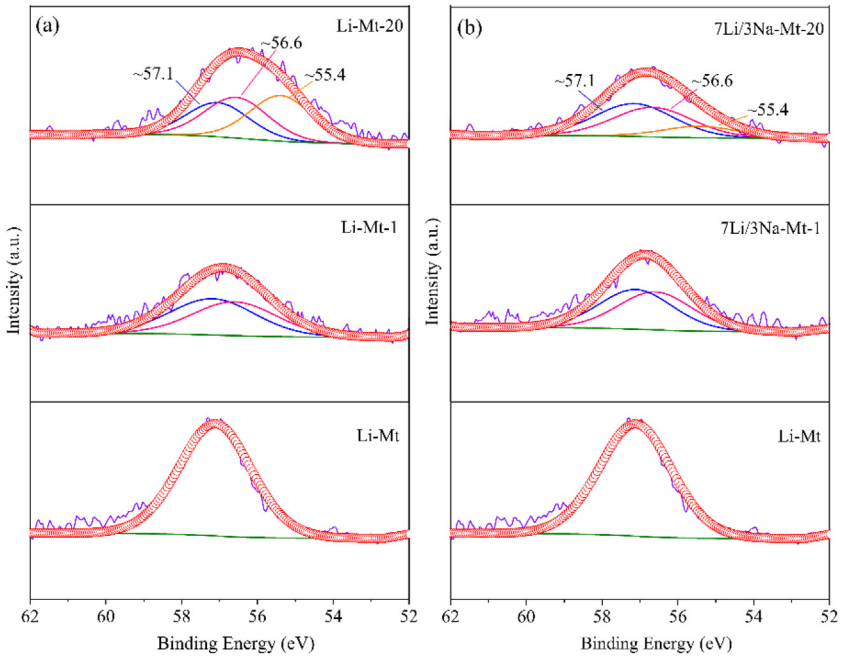

Fig. 4. The high resolution of Li1s XPS spectra of Li-Mt-s (a) and 7Li/3Na-Mt-s (b), respectively. Li-Mt represents Mt treated with molten $LiNO_3$ at 260 °C for 5 min. Li-Mt-1 and Li-Mt-20 represent Mt treated with molten $LiNO_3$ at 260 °C for 1 and 20 h, respectively. 7Li/3Na-Mt-1 and 7Li/3Na-Mt-20 represent Mt treated with molten $LiNO_3$-$NaNO_3$ mixture at 260 °C for 1 and 20 h, respectively.

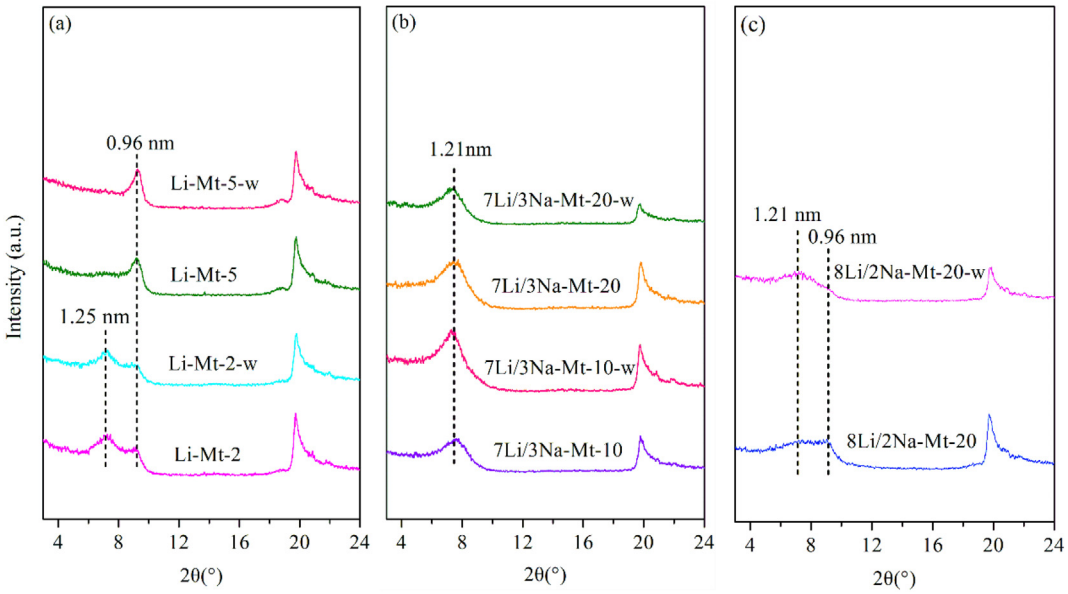

Fig. 5. The XRD patterns of hydrated and then re-dried samples of Li-Mt-s (a), 7Li/3Na-Mt-s (b), and 8Li/2Na-Mt-s (c), respectively. Li-Mt-2-w, Li-Mt-5-w, 7Li/3Na-Mt-10-w, 7Li/3Na-Mt-20-w, and 8Li/2Na-Mt-20-w represent the hydrated and then re-dried samples of Li-Mt-2, Li-Mt-5, 7Li/3Na-Mt-10, 7Li/3Na-Mt-20, and 8Li/2Na-Mt-20, respectively.

during thermal treatment. Therefore, the locations of fixed Li^+ ions in the layers of RC-Mt are further validated by XPS.

3.5. The swelling capacity of collapse layers in RC-Mt

In order to investigate whether the collapse layers in the RC-Mt can be expanded, the hydration experiment was carried out. The XRD patterns of samples were recorded (Fig. 5). After hydration at room temperature, the collapsed Mt layers in Li-Mt-s (treated with molten $LiNO_3$) failed to expand (Fig. 5a). Specifically, the d_{001} reflection corresponding to 0.96 nm for Li-Mt-2-w and Li-Mt-5-w was still observed, and the intensity has little change. This is in agreement with the XRD analysis of Komadel et al. (2002), where the collapse layers in RC-Mt was non-swelling. Moreover, compared to that of RC-Mt (e.g., Li-Mt-2 and Li-Mt-5), no changes in CEC values of Li-Mt-2-w and Li-Mt-5-w were observed (Table S1), which further indicates the irreversible of charge reduction. After hydration, a single d_{001} reflection corresponding to 1.21 nm for 7Li/3Na-Mt-10-w and 7Li/3Na-Mt-20-w was shown (Fig. 5b), and the full width at half maximum (FWHM) values of the (001) reflections were lower than those of the samples without being mixed with distilled water again (Table S2). These results indicate that the layer structure of 7Li/3Na-Mt-s-w becomes more ordered in the *c* axis direction. Moreover, a broader and less intense basal reflection corresponding to 0.96 nm was observed for 8Li/2Na-Mt-20-w (Fig. 5c), which indicates that some of the collapsed Mt layers in 8Li/2Na-Mt-20 (having a lower CEC value) are expanded. This result should be ascribed to the existence of Na^+ ions within the interlayer spaces. Thus, water molecules can reach the interlayer spaces and hydrate the Na^+ ions. Therefore, the existence of Na^+ ions within the interlayer spaces can well maintain the swelling capacity of Mt.

To further confirm the molten salts mixture in maintaining the interlayer spaces, Li-Mt-2 and 7Li/3Na-Mt-10, which have the same CEC, were specifically compared. The layers of Li-Mt-2 collapsed during the thermal treatment (Fig. 1a), and the collapse layers in its counterpart after hydration (Li-Mt-2-w) was non-swelling (Fig. 5a), whereas the interlayer spaces of 7Li/3Na-Mt-10 was well maintained (Fig. 1b), and after hydration, its layer structure became more ordered (Fig. 5b). Such differences should be determined by the existence of Na^+ in the interlayer spaces (Bergaya et al., 1979). However, the FTIR spectra and XPS spectra of Li-Mt-2 and 7Li/3Na-Mt-10 and their hydrated counterparts showed no obvious differences (Fig. S2 and S3), this result is attributed to the unchanged distributed locations of the migrated Li^+ (e.g., the hexagonal cavities on tetrahedral sheets and the vacant sites on octahedral sheets) for Li-Mt-2 and 7Li/3Na-Mt-10 and their hydrated samples.

The above results showed that after the RC-Mt was mixed with water again, the collapsed layers in the samples treated with molten $LiNO_3$ cannot be expanded, while some of the collapsed layers in the samples treated with molten $LiNO_3$-$NaNO_3$ mixture can be expanded. Therefore, due to the existence of Na^+ ions within the interlayer spaces, RC-Mt could provide more accessible interlayer spaces.

3.6. Mechanism and the importance of preparing RC-Mt via molten salts treatment

According to the above results, the mechanisms for reducing the layer charges of Mt treated with molten $LiNO_3$ and molten $LiNO_3$-$NaNO_3$ mixture are deduced. When Ca-Mt is completely covered with excess molten $LiNO_3$ or $LiNO_3$-$NaNO_3$ mixture, the ionized Li^+ and Na^+ ions can rapidly exchange with Ca^{2+} ions. Moreover, the hydrated cations within the interlayer spaces of Mt are dehydrated during the heating process (Chen et al., 2017), and the dehydrated Li^+ ions can directly migrate into the Mt layers at high temperature to neutralize the layer charge. In addition, in the molten $LiNO_3$ system, the inhomogeneous migration of Li^+ ions into the layers causes the inhomogeneous collapse of Mt layers. While in the molten $LiNO_3$-$NaNO_3$ mixture system, although most of the Li^+ ions migrated into the layers, the Na^+ ions (with large radius) can act as 'pillars' to restrict the interlayer spaces from collapse (Bergaya et al., 1979).

The conventional methods for preparing RC-Mt generally need to first exchange small cations into the interlayer spaces of Mt and then heat the resulting samples with desired temperature and time (Madejová et al., 1999; Zemanová et al., 2006). To prevent the collapse of Mt layers, a large cation needs to be further exchanged into the interlayer spaces of Mt (Pálková et al., 2009; Luo et al., 2014). These methods are complex and time-consuming, and also produce a large amount of wastewater. On the other hand, the results of this study clearly showed that RC-Mt can be conveniently prepared via a facile one-pot synthesis strategy, i.e., heating the mixture of Mt and molten $LiNO_3$. Moreover, the interlayer spaces of Mt can also be maintained by

replacing a proper amount of $LiNO_3$ with $NaNO_3$ (i.e., using the molten $LiNO_3$-$NaNO_3$ mixture). After RC-Mt was mixed with water again, some of the collapsed layers in the samples treated with molten $LiNO_3$-$NaNO_3$ mixture can be expanded. As such, this method is much simpler and more efficient and can be potentially applied for the large-scale production of RC-Mt.

4. Conclusions

In summary, RC-Mt was successfully prepared via a one-pot synthesis strategy, which involved heating the mixture of Mt and molten salts. When Mt is treated with molten $LiNO_3$, Ca^{2+} ions within the interlayer spaces of Mt can be rapidly exchanged by Li^+ ions, and then Li^+ ions can directly migrate into the Mt layer to neutralize the layer charge. In addition, the inhomogeneous migration of Li^+ ions into the layers causes the inhomogeneous collapse of Mt layers. On the other hand, by partly replacing $LiNO_3$ with $NaNO_3$, the interlayer spaces of Mt can be well maintained, and some of the collapsed layers in the samples can be expanded, and these results should be ascribed to the existence of Na^+ within the interlayer spaces. Moreover, when Mt is treated with molten $LiNO_3$, layer charge decreases rapidly, while the partial replacement of $LiNO_3$ by $NaNO_3$ could weaken the efficiency of reduction for layer charge. The hexagonal cavities of tetrahedral sheets and vacant octahedral sites on Mt layers are the locations for fixing Li^+ ions. Overall, this work provided a facile, fast, and environmentally friendly approach for preparing RC-Mt, which would greatly contribute to the large-scale preparation of RC-Mt.

Declaration of Competing Interest

The authors declare that they have no known competing financial interests or personal relationships that could have appeared to influence the work reported in this paper.

Acknowledgments

This work was financially supported by the National Natural Science Foundation of China (41572031), the Guangdong Special Support Program (2017TX04Z243), the National Science Fundation for Distinguished Young Scholars (41825003), CAS Interdisciplinary Innovation Team (JCTD-2019-15), and Youth Innovation Promotion Association CAS. The authors also thank Professor Y. F. Xi from Queensland University of Technology for revising the manuscript, X. Liu from Sun Yat-sen university for revising the manuscript, and S. Y. Li from Guangzhou Institute of Geochemistry, Chinese Academy of Sciences for the calculation of the structural formula for Mt. This is contribution No.IS-2792 from GIGCAS.

Appendix A. Supplementary data

Supplementary data to this article can be found online at https://doi.org/10.1016/j.clay.2019.105429.

References

Alvero, R., Alba, M.D., Castro, M.A., Trillo, J.M., 1994. Reversible migration of lithium in montmorillonites. J. Phys. Chem. 98, 7848–7853.
Barrientos-Velázquez, A.L., Marroquin Cardona, A., Liu, L., Phillips, T., Deng, Y.J., 2016. Influence of layer charge origin and layer charge density of smectites on their aflatoxin adsorption. Appl. Clay Sci. 132-133, 281–289.
Bergaya, F., Cruz, M.I., Gatineau, L., Fripiat, J.J., 1979. Adsorption of alcohols by smectites. I. Distinction between internal and external surfaces. Clay Miner. 14, 249–258.
Bergaya, F., Lagaly, G., 2013. Chapter 1-general introduction: clays, clay minerals, and clay science. In: Bergaya, F., Lagaly, G. (Eds.), Developments in Clay Science. Elsevier, pp. 1–19 5 A.
Bujdák, J., Janek, M., Madejová, J., Komadel, P., 2001. Methylene blue interactions with reduced-charge smectites. Clay Clay Miner. 49, 244–254.
Chen, Q.Z., Zhu, R.L., Ma, L.Y., Zhou, Q., Zhu, J.X., He, H.P., 2017. Influence of interlayer species on the thermal characteristics of montmorillonite. Appl. Clay Sci. 135, 129–135.
Chen, Q.Z., Liu, S.H., Zhu, R.L., Wu, D.C., Fu, H.Y., Zhu, J.X., He, H.P., 2018. Clay minerals derived nanostructured silicon with various morphology: Controlled synthesis, structural evolution, and enhanced lithium storage properties. J. Power Sources 405, 61–69.
Chen, Q.Z., Zhu, R.L., He, Q.Z., Liu, S.H., Wu, D.C., Fu, H.Y., Du, J., Zhu, J.X., He, H.P., 2019. In-situ synthesis of silicon flake/nitrogen-doped graphene-like carbon composite from organoclay for high-performance lithiumion battery anode. Chem. Commun. 55, 2644–2647.
Chorom, M., Rengasamy, M., 1996. Effect of heating on swelling and dispersion of different cationic forms of a smectite. Clay Clay Miner. 6, 783–790.
Christidis, G.E., Blum, A.E., Eberl, D.D., 2006. Influence of layer charge and charge distribution of smectites on the flow behaviour and swelling of bentonites. Appl. Clay Sci. 34, 125–138.
Clementz, D.M., Mortland, M.M., 1974. Propertites of reduced charge Montmorillonite: tetra-alkylammonium ion exchange forms. Clay Clay Miner. 22, 223–229.
Czímerová, A., Iyi, N., Bujdák, J., 2008. Fluorescence resonance energy transfer between two cationic laser dyes in presence of the series of reduced-charge montmorillonites: effect of the layer charge. J. Colloid Interface Sci. 320, 140–151.
Deng, X., Zhao, B., Zhu, L., Shao, Z.P., 2015. Molten salt synthesis of nitrogen-doped carbon with hierarchical pore structures for use as high-performance electrodes in supercapacitors. Carbon. 93, 48–58.
Ebina, T., Iwasaki, T., Chatterjee, A., 1999. XPS and DFT study on the migration of lithium in Montmorillonite. Clay Sci. 10, 569–581.
Gil, A., Vicente, M.A., Gandia, L.M., 2000. Main factors controlling the texture of zirconia and alumina pillared clays. Microporous Mesoporous Mater. 34, 115–125.
Hu, Z.M., Xiao, X., Jin, H.Y., Li, T.Q., Chen, M., Liang, Z., Guo, Z.F., Li, J., Wan, J., Huang, L., Zhang, Y.R., Feng, G., Zhou, J., 2017. Rapid mass production of two-dimensional metal oxides and hydroxides via the molten salts method. Nat. Commun. 8, 15630.
Jaynes, W.F., Traina, S.J., Bigham, J.M., 1992. Preparation and characterization of reduced-charge hectorites. Clay Clay Miner. 40, 397–404.
Komadel, P., 2003. Chemically modified smectites. Clay Miner. 38, 127–138.
Komadel, P., Hrobáriková, J., Smrčok, L., Koppelhuber-Bitschnau, B., 2002. Hydration of reduced-charge montmorillonite. Clay Miner. 37, 543–550.
Komadel, P., Madejová, J., Hrobáriková, J., Janek, M., Bujdák, J., 2003. Fixation of Li^+ cations in montmorillonite upon heating. Solid State Phenom. 90–91, 497–502.
Kuligiewicz, A., Derkowski, A., Emmerich, K., Christidis, G.E., Tsiantos, C., Gionis, V., Chryssikos, G.D., 2015. Measuring the layer charge of dioctahedral smectite by O-D vibrational spectroscopy. Clay Clay Miner. 63, 443–456.
Luo, Z.X., Gao, M.L., Ye, Y., Yang, S.F., 2014. Wettability studies of reduced-charge montmorillonites modified by quaternary ammonium salts using capillary rise test. Powder Technol. 266, 167–174.
Luo, Z.X., Gao, M.L., Ye, Y., Yang, S.F., 2015. Modification of reduced-charge montmorillonites by a series of Gemini surfactants: Characterization and application in methyl orange removal. Appl. Surf. Sci. 324, 807–816.
Ma, J.F., Huang, D.Q., Zhang, W.Y., Zou, J., Kong, Y., Zhu, J.X., Komarneni, S., 2016. Nanocomposite of exfoliated bentonite/g-C3N4/Ag_3PO_4 for enhanced visible-light photocatalytic decomposition of Rhodamine B. Chemosphere 162, 269–276.
Madejová, J., Arvaiová, B., Komadel, P., 1999. FTIR spectroscopic characterization of thermally treated Cu^{2+}, Cd^{2+}, and Li^+ montmorillonites. Spectrochim. Acta. Part A. 55, 2467–2476.
Madejová, J., Bujdák, J., Petit, S., Komadel, P., 2000. Effects of chemical composition and temperature of heating on the infrared spectra of Li-saturated dioctahedral smectites. (I) Mid-infrared region. Clay Miner. 35, 739–751.
Madejová, J., Pálková, H., Komadel, P., 2006. Behaviour of Li^+ and Cu^{2+} in heated montmorillonite: evidence from far-, mid-, and near-IR regions. Vib. Spectrosc. 40, 80–88.
Mishra, B.G., Rao, G.R., 2004. Physicochemical and catalytic properties of Zr-pillared montmorillonite with varying pillar density. Microporous Mesoporous Mater. 70, 43–50.
Ormerod, E.C., Newman, A.C.D., 1983. Water sorption on Ca-saturated clays: II. Internal and external surfaces of montmorillonite. Clay Miner. 18, 289–299.
Pálková, H., Madejová, J., Righi, D., 2003. Acid dissolution of reduced-charge Li- and Ni-montmorillonites. Clay Clay Miner. 51, 133–142.
Pálková, H., Madejová, J., Komadel, P., 2009. The effect of layer charge and exchangeable cations on sorption of biphenyl on montmorillonites. Cent. Eur. J. Chem. 7, 494–504.
Purnell, J.H., Yun, L.M., 1993. Ionic migration and charge reduction in Ni^{2+}-, Co^{2+}- and Zn^{2+}-exchanged Texas montmorillonite. Catal. Lett. 18, 235–241.
Ruan, X.X., Zhu, L.Z., Chen, B.L., 2008. Adsorptive characteristics of the siloxane surfaces of reduced-charge bentonites saturated with tetramethylammonium cation. Environ. Sci. Technol. 42, 7911–7917.
Skoubris, E.N., Chryssikos, G.D., Christidis, G.E., 2013. Structural characterization of reduced-charge montmorillonites. Evidence based on FTIR spectroscopy, thermal behavior, and layer-charge systematics. Clay Clay Miner. 61, 83–97.
Srasra, E., Bergaya, F., Friprat, J.J., 1994. Infrared spectroscopy study of tetrahedral and octahedral substitutions in an interstratified illite-smectite clay. Clay Clay Miner. 42, 237–241.
Sun, G.D., Zhang, G.H., Chou, K.C., 2019. Preparation of Mo nanoparticles through hydrogen reduction of commercial MoO_2 with the assistance of molten salt. Int. J. Refrct. Met. Hard Mater. 78, 68–75.
Sychev, M., Shubina, T., Rozwadowski, M., Sommen, A.P.B., De Beer, V.H.J., Van Santen, R.A., 2000. Characterization of the microporosity of chromia- and titania-pillared montmorillonites differing in pillar density. I. Adsorption of nitrogen. Microporous Mesoporous Mater. 37, 187–200.
Theng, B., K, G., Hayashi, S., Soma, M., Seyama, H., 1997. Nuclear magnetic resonance

and X-RAY photoelectron spectroscopic investigation of lithium migration in montmorillonite. Clay Clay Miner. 45, 718–723.
Wang, Y.B., Su, X.L., Lin, X.Q., Zhang, P., Wen, K., Zhu, J.X., He, H.P., 2015. The non-micellar template model for porous clay heterostructures: a perspective from the layer charge of base clay. Appl. Clay Sci. 116–117, 102–110.
White, J.L., 1954. Reaction of molten salt with layer lattice silicates. Nature. 174, 799–800.
Wu, L.M., Liao, L.B., Lv, G.C., Qin, F.X., Li, Z.H., 2014. Microstructure and process of intercalation of imidazolium ionic liquids into montmorillonite. Chem. Eng. J. 236, 306–313.
Zemanová, M., Link, G., Takayama, S., Nüesch, R., Janek, M., 2006. Modification of layer charge in smectites by microwaves. Appl. Clay Sci. 32, 271–282.
Zhang, Y.Y., Wu, J.Q., Wang, W.L., Ding, J.J., Lu, J.F., 2019. Experimental and numerical studies on molten salt migration in porous system with phase change. Int. J. Heat Mass Tran. 129, 397–405.
Zhou, C.H., 2011. An overview on strategies towards clay-based designer catalysts for green and sustainable catalysis. Appl. Clay Sci. 53, 87–96.
Zhou, C.H., Li, C.J., Gates, W.P., Zhu, T.T., Yu, W.H., 2019. Co-intercalation of organic cations/amide molecules into montmorillonite with tunable hydrophobicity and swellability. Appl. Clay Sci. 179, 105157.
Zhu, L.Z., Zhu, R.L., Xu, L.H., Ruan, X.X., 2007. Influence of clay charge densities and surfactant loading amount on the microstructure of CTMA–montmorillonite hybrids. Colloids Surf. A Physicochem. Eng. Asp. 304, 41–48.
Zhu, R.L., Zhu, L.Z., Xu, L.H., 2007b. Sorption characteristics of CTMA–bentonite complexes as controlled by surfactant packing density. Colloid Surf. A. 294, 221–227.
Zhu, R.L., Zhao, J.B., Ge, F., Zhu, L.F., Zhu, J.X., Tao, Q., He, H.P., 2014. Restricting layer collapse enhances the adsorption capacity of reduced-charge organoclays. Appl. Clay Sci. 88-89, 73–77.
Zhu, R.L., Chen, Q.Z., Zhou, Q., Xi, Y.F., Zhu, J.X., He, H.P., 2016. Adsorbents based on montmorillonite for contaminant removal from water: a review. Appl. Clay Sci. 123, 239–258.
Zitnan, M., Szöcs, V., Janek, M., Bugar, I., Bdzoch, J., Palszegi, T., Link, G., Velic, D., 2009. Fluorescence dynamics of Coumarin C522 on reduced-charge montmorillonite in aqueous dispersion. Langmuir. 25, 6800–6807.